Ultrafast Charge-Transfer Dynamics at the Boron Subphthalocyanine Chloride/C60 Heterojunction: Comparison between Experiment and Theory

ARTICLE *in* JOURNAL OF PHYSICAL CHEMISTRY LETTERS · JANUARY 2015

Impact Factor: 7.46 · DOI: 10.1021/jz502278k

8 AUTHORS, INCLUDING:

Myeong H Lee
The University of Warwick
30 PUBLICATIONS **339** CITATIONS
SEE PROFILE

Andrew Niedringhaus
University of Michigan
4 PUBLICATIONS **8** CITATIONS
SEE PROFILE

Max Shtein
University of Michigan
86 PUBLICATIONS **2,577** CITATIONS
SEE PROFILE

THE JOURNAL OF PHYSICAL CHEMISTRY Letters

Letter

pubs.acs.org/JPCL

Ultrafast Charge-Transfer Dynamics at the Boron Subphthalocyanine Chloride/C_{60} Heterojunction: Comparison between Experiment and Theory

Daniel E. Wilcox,[†] Myeong H. Lee,[‡,∥,○] Matthew E. Sykes,[⊥] Andrew Niedringhaus,[†] Eitan Geva,[‡] Barry D. Dunietz,[∥] Max Shtein,[⊥,#,▽] and Jennifer P. Ogilvie*[,†,§]

[†]Department of Physics, University of Michigan, 450 Church Street, Ann Arbor, Michigan 48109, United States

[‡]Department of Chemistry and [§]Biophysics Program, University of Michigan, 930 North University Avenue, Ann Arbor, Michigan 48109, United States

[∥]Department of Chemistry, Kent State University, 214 Williams Hall, Kent, Ohio 44242, United States

[⊥]Department of Materials Science and Engineering, [#]Department of Macromolecular Science and Engineering, and [▽]Department of Chemical Engineering, University of Michigan, 2300 Hayward Street, Ann Arbor, Michigan 48109, United States

Supporting Information

ABSTRACT: Photoinduced charge-transfer (CT) processes play a key role in many systems, particularly those relevant to organic photovoltaics and photosynthesis. Advancing the understanding of CT processes calls for comparing their rates measured via state-of-the-art time-resolved interface-specific spectroscopic techniques with theoretical predictions based on first-principles molecular models. We measure charge-transfer rates across a boron subphthalocyanine chloride (SubPc)/C_{60} heterojunction, commonly used in organic photovoltaics, via heterodyne-detected time-resolved second-harmonic generation. We compare these results to theoretical predictions based on a Fermi's golden rule approach, with input parameters obtained using first-principles calculations for two different equilibrium geometries of a molecular donor−acceptor in a dielectric continuum model. The calculated rates (~2 ps^{-1}) overestimate the measured rates (~0.1 ps^{-1}), which is consistent with the expectation that the calculated rates represent an upper bound over the experimental ones. The comparison provides valuable understanding of how the structure of the electron donor−acceptor interface affects the CT kinetics in organic photovoltaic systems.

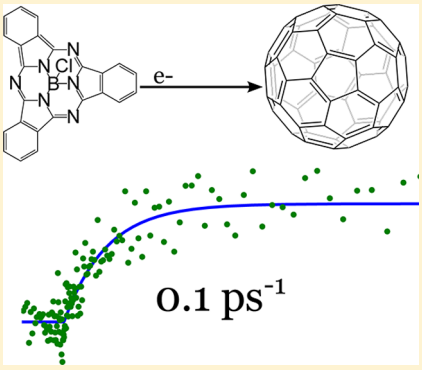

Photoinduced charge transfer is a key component of many chemically, biologically, and technologically relevant processes, including photocatalysis, photovoltaics, and photosynthesis. In the case of organic photovoltaics, light absorption by the electron donor or acceptor layer eventually triggers the creation of a charge-separated state across the donor/acceptor interface, which upon dissociation of the interfacial electron−hole pair gives rise to an electrical current. Similarly, photosynthetic reactions correspond to transforming the energy of the absorbed photons into that of charge-separated states, which can drive life-sustaining reactions such as water splitting.[1]

A variety of experimental methods have been used to measure charge-transfer rates. For example, ultrafast transient absorption (also called pump−probe or photoinduced absorption) and time-resolved fluorescence (or photoluminescence) spectroscopies have been used to track spectral signatures attributed to charge-transfer or charge-separated states.[2−6] Near-infrared transient absorption in organic photovoltaic systems is commonly attributed to charge-transfer states.[2−4] Unfortunately, charge-transfer states are often dark.[7] Furthermore, the signal obtained via such methods as transient absorption pump−probe spectroscopy corresponds to a third-order optical response, which is dominated by the bulk material. This makes it difficult to resolve contributions from interfacial charge-transfer and charge-separation processes.[8]

Recently, a number of groups have employed time-resolved second harmonic generation (TRSHG) as a more direct way of probing charge-transfer dynamics in organic photovoltaic materials.[8−10] Importantly, the second-harmonic generation (SHG) signal vanishes in centrosymmetric materials,[11] thereby making it insensitive to bulk processes and highly sensitive to processes that occur at the donor/acceptor interface, where the centrosymmetry is broken. TRSHG can be used to provide an interface-specific measure of charge-transfer using electric-field-induced second-harmonic generation (EFISH).[8] The latter is a four-wave mixing nonlinear optical phenomenon, where a quasi-static electric field E_{DC} allows an optical signal P^{NL} to be produced as the second harmonic of a probe pulse: P^{NL} =

Received: October 28, 2014
Accepted: January 16, 2015

DOI: 10.1021/jz502278k
J. Phys. Chem. Lett. 2015, 6, 569−575

$\chi^{(3)}E_{DC}E^2_{probe}$. Charge transfer at the interface then creates the quasi-static field E_{DC}, which leads to a measurable EFISH signal.

The electronic structure of excited charge-transfer states of complex molecular systems can be calculated by high-quality many-body expansion methods, for example, using the GW approximation with the Bethe–Salpeter (BSE) equation.[12−15] However, the prohibitive computational cost of such techniques requires using more feasible alternatives such as time-dependent density functional theory (TD-DFT). Indeed, implemented with recently developed range-separated hybrid (RSH) functionals,[16−21] TD-DFT was shown to reproduce GW-BSE energies.[13,22] Furthermore, combining TD-DFT/RSH with a description of the electrostatic environment as a polarizable dielectric continuum was recently shown to yield charge-transfer states whose energies are in good agreement with experiment.[23−25]

Most computational studies on charge-transfer rates in organic photovoltaic materials[26−29] are based on the semiclassical Marcus picture of photoinduced charge-transfer.[30−32] However, Marcus theory relies on a number of simplifying assumptions that do not hold in general when considering organic semiconducting materials.[33−35] Marcus theory can be derived from the more general fully quantum-mechanical Fermi's golden rule (FGR) expression for the charge-transfer rate constant.[36−40] However, doing so requires imposing both the high-temperature and short time limits. Importantly, because charge transfer in organic photovoltaic materials may occur in the (far) inverted regime, nuclear tunneling can become a dominant mechanism for electronic transitions due to enhanced overlap between the nuclear wave functions.[41,42] Furthermore, the previously mentioned short-time expansion may not be valid. Indeed, we have recently demonstrated the importance in using the less approximate fully quantum-mechanical FGR expression for calculating charge-transfer rates. The calculated FGR rate constants thus obtained were found to be in good agreement with corresponding experimental values, whereas the classical Marcus rate constants were found to significantly underestimate the experimental values.[33−35]

We study a model system of an organic photovoltaic heterojunction, in which boron subphthalocyanine chloride (SubPc) and C_{60} function as the electron donor and acceptor, respectively. Upon photoexcitation, the SubPc transfers an electron to the C_{60}, generating a charge-transfer state. To directly observe the charge transfer, we used our recently developed heterodyne-detected TRSHG (hTRSHG) spectroscopy.[43] Adding heterodyne detection to TRSHG decreases sensitivity to read noise, dark current, and stray light. It also allows both the amplitude and the phase of the SHG to be directly detected, which can aid physical understanding, for example, providing information about molecular orientations or the direction of charge transfer.[43]

A detailed description of our hTRSHG setup was previously published.[43] For this experiment, a 580 nm pump pulse created a subpopulation of excited molecules, after which an 800 nm probe pulse was used to probe the electric field at the interface, and thereby charge transfer, as a function of the time delay between pump and probe pulses. We found that very low laser fluences were necessary to avoid higher-order processes such as exciton–exciton annihilation and laser-induced aging, as discussed in detail in the Supporting Information. We therefore reduced the probe fluence to 50 $\mu J/cm^2$ and the pump fluence to 2 $\mu J/cm^2$; we estimate that under these conditions the pump

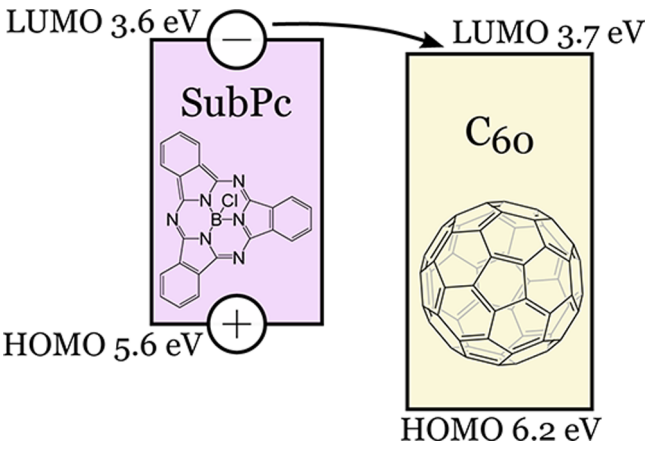

Figure 1. Depiction of the charge-transfer process under investigation. Boron subphthalocyanine chloride (SubPc) absorbs light, creating a bound electron–hole pair or exciton. In proximity to a C_{60} molecule, the electron is donated to the C_{60}, generating a charge-transfer state.

excites ∼0.1% of the SubPc molecules. Three types of samples were prepared on an ultrasmooth c-cut sapphire wafer (Precision Micro-Optics): (1) a 3 nm film of SubPc capped by 20 nm of C_{60}; (2) a neat 20 nm film of C_{60}; and (3) a neat 3 nm film of SubPc. Films were deposited onto room-temperature substrates using vacuum thermal evaporation at a pressure below 5×10^{-7} Torr and at deposition rates of 1 and 0.5 Å/s for C_{60} and SubPc, respectively. Samples were encapsulated under a pure nitrogen atmosphere using a BK7 window and solvent-free UV-cured epoxy to prevent oxygen- and moisture-induced degradation.

Figure 2 shows the pump and probe laser spectra and the samples' linear absorption spectra. The 580 nm pump

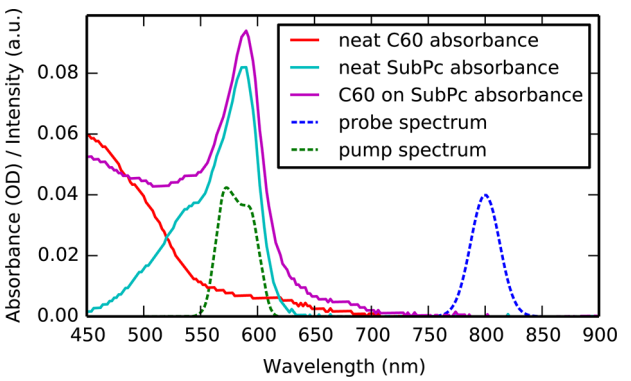

Figure 2. Laser spectra and samples' absorbance. The probe pulse, centered at 800 nm, is well-separated from main absorption. The pump pulse, centered at 580 nm, maximizes absorption from the SubPc.

wavelength primarily excites the SubPc molecules. The probe pulse is well-separated from primary absorptions and so primarily interacts nonlinearly, producing SHG. There may be some resonance between the probe and low-lying charge-transfer absorptions, but that should not affect our interpretation of the charge-transfer kinetics. Here we report two representative sets of bilayer charge-transfer data, taken on different days, with fresh samples. A separate hTRSHG trace was taken with the probe pulse in the s and p polarizations. As expected, a p-polarized probe pulse yielded the strongest SHG

DOI: 10.1021/jz502278k
J. Phys. Chem. Lett. 2015, 6, 569−575

signals.[9,11] We only measured the p-polarized component of the signal because, as expected, that was the overwhelmingly dominant component of the signal.[8,11] We best-fit the data using a single-exponential model, with the same rate k for both polarizations

$$S_i(t) = A_i + B_i\theta(t)[1 - \exp(-kt)] \quad (1)$$

Here $S_i(t)$ represents the measured complex hTRSHG signal as a function of polarization, i, and pump−probe relative time delay, t. A_i represents the ground-state signal ($t < 0$) and B_i represents the change in SHG due to the presence of the pump, in the limit of large t. Both A_i and B_i are complex and depend on the polarization i. $\theta(t)$ is the Heaviside step function. k is the (real) rate constant, and does not depend on polarization. We used the curve_fit function in the open-source scipy.optimize module[44] to perform the fitting. The unknowns in the fit were A_i, B_i, and k. The measured data and their fits are shown in Figure 3 by plotting the principal projection $\mathcal{P}$ of the data onto

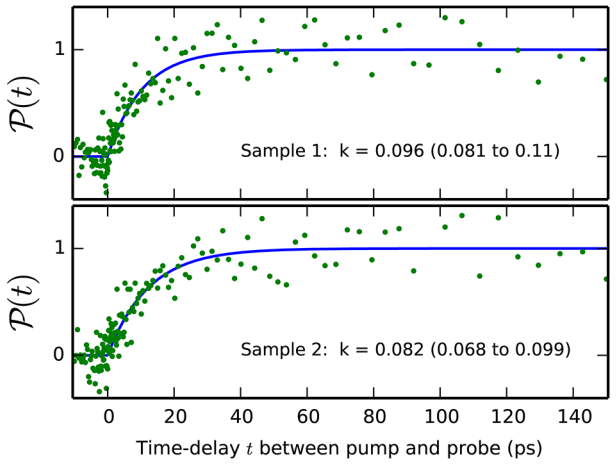

Figure 3. Measured and fitted principal projection $\mathcal{P}$ of the hTRSHG data. Green dots, measured data. Blue line, fitted single-exponential curve. The measurement was repeated on different days with fresh samples; the fitted charge-transfer rate k is shown in ps^{-1} with 95% confidence intervals. Top subfigure, bilayer sample 1; bottom subfigure, bilayer sample 2. Data from neat films not shown due to absence of dynamics.

the $\vec{A}$−$\vec{B}$ line, as defined in the Supporting Information. This projection starts at 0 before time zero and converges to 1 in the limit of large pump−probe time delay. We found that this projection captured the majority of the information in the data; the data-components orthogonal to this projection were dominated by noise. The fitted time constants and associated confidence intervals for the bilayer films are shown in Figure 3, indicating that the charge-transfer rate is $k \approx 0.1$ ps^{-1}, reasonably consistently across the two bilayer films. This rate is likely an average charge-transfer rate because different individual molecules in different local environments are expected to have different charge-transfer rates. Control studies of neat films showed no changes in the SHG due to the pump, indicating that no charge transfer occurred.

For our theoretical calculations, we considered two representative molecular models of likely interfacial configurations based on optimized donor−acceptor dimers in a dielectric continuum model, namely, the hollow and on-top configurations, shown in the inset of Figure 4.[34] While donor−acceptor trimers have been shown to yield significantly different

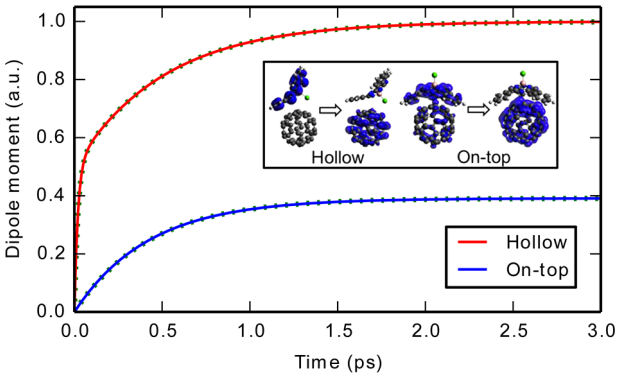

Figure 4. Calculated expected electric dipole moment $\mu(t)$ as a function of time for two SubPc/C_{60} interface configurations, showing the occupancy transferring from the bright absorbing states to the dark charge transfer states. Red solid line, hollow configuration; blue solid line, on-top configuration. Green dotted lines, best-fit curves. Inset shows the detachment and attachment of electron densities upon photoexcitation, indicating the electron transfer from SubPc to C_{60}. The hollow best-fit curve was biexponential, with a 51 ps^{-1} component and a 2.0 ps^{-1} component. The on-top best-fit curve was single-exponential, showing an average charge-transfer rate of 2.3 ps^{-1}.

simulated results than dimers for a copper phthalocyanine (CuPc)/C_{60} heterojunction,[10,35] we do not expect the difference between dimers and trimers to be so large in the SubPc/C_{60} system. While CuPc exhibits strong planar stacking and therefore strong coupling between CuPc molecules, SubPc packs poorly due to its irregular shape; therefore, we do not expect such strong coupling between SubPc molecules. In addition to reducing the effect of using trimers in the simulation, we also expect SubPc's poor packing to affect interfacial donor−acceptor geometries in actual thin films. In the interface, the molecules likely deviate from optimal geometries, where they are expected to be less tightly packed. We therefore expect the calculated charge-transfer rates to serve as upper bounds to experimentally measured rates.

The photoinduced charge transfer involves coupling a dark charge-transfer state to an absorbing bright state. In the system considered here, the electron is transferred from SubPc to C_{60}, as illustrated by the detachment and attachment electron densities shown in Figure 4. However, it should be noted that some of the donor-excited states of the on-top configuration already exhibit charge-transfer character due to some delocalization across the donor and acceptor regions.

Because a TRSHG measurement tracks the electric field at the interface, a comparison between our experimental and computational results can be made by following the time-dependent electric dipole moment, $\mu(t)$

$$\mu(t) = \sum_i \mu_i P_i(t) \quad (2)$$

Here $P_i(t)$ is the evolving occupancy of excited state i, and the electric dipole moment μ_i for state i is given by $\mu_i = q^i_D|\mathbf{r}^i_D - \mathbf{r}^i_A|$, where $q^i_D = (= -q^i_A)$ is the total Mulliken charge on donor (D) molecule obtained from the TD-DFT calculation and $\mathbf{r}^i_{D/A}$ is the center of charge of D/A molecules defined by

$$\mathbf{r}^i_{D/A} = \frac{\sum_{j\in D/A} |q^i_j|\mathbf{r}^i_j}{\sum_{j\in D/A} |q^i_j|} \quad (3)$$

DOI: 10.1021/jz502278k
J. Phys. Chem. Lett. 2015, 6, 569−575

The excited states' occupancies, $P_i(t)$, were obtained by solving a Master equation under the assumption that the initial state is dominated by states that absorb within the pump bandwidth

$$\dot{P}_i(t) = \sum_{j\neq i} [-k_{ji}P_i(t) + k_{ij}P_j(t)]$$
$$\text{where } P_i(t=0) \equiv \frac{|OS_i|}{\sum_j |OS_j|}, \quad \sum_i P_i(t) = 1 \tag{4}$$

Here k_{ji} is the FGR rate constant for the electronic transition from state i to state j, and OS_i is the oscillator strength of excited state i. We used an effective oscillator strength of zero ($OS_i = 0$) for all of the charge-transfer states, including the bright ones, because our pump laser pulse was relatively narrowband and not resonant with the charge-transfer states.

The FGR rate constant for an electronic transition from the electronic state b to a is given by[36−40]

$$k_{a\leftarrow b} = \frac{|V_{ba}|^2}{\hbar^2}\int_{-\infty}^{\infty} \mathrm{d}t\ \mathrm{e}^{i\omega_{ba}t}F(t) \tag{5}$$

where $F(t) = \exp[\sum_{\alpha=1}^{N}[-S_\alpha(2n_\alpha + 1) + S_\alpha[(n_\alpha + 1)\mathrm{e}^{-i\omega_\alpha t} + n_\alpha \mathrm{e}^{i\omega_\alpha t}]]]$. Here V_{ba}, $\omega_{ba} = (E_b - E_a)/\hbar$, $\{\omega_\alpha\}$ and $\{n_\alpha = [\mathrm{e}^{((\hbar\omega_\alpha)/(k_B T))} - 1]^{-1}\}$ are the electronic coupling coefficient, transition frequency, normal-mode frequencies, and thermal equilibrium occupancies, respectively. The Huang−Rhys factor, S_ω[45] represents the electron-vibration coupling strength, which is obtained by projecting the displacement between the initial and final equilibrium geometries onto the normal modes of the ground state.

Density functional theory (DFT) was employed for the ground-state, time-dependent density functional theory (TD-DFT) for excited states, and charge-constrained density functional theory (C-DFT)[46] for determining the CT state geometry and energy as affected by the electrostatic environment.[34] All of the calculations were performed with the 6-31G* basis set. Geometry optimization of the ground and the CT states was based on the ωB97X-D dispersion-corrected functional, designed for accurately describing noncovalent interactions.[47,48] The optimal geometries of the $\pi-\pi^*$ excited state were assumed to be the same as the ground-state optimal geometry. TD-DFT gas-phase calculations were based on the range-separated hybrid functional of Baer−Neuhauser−Livshits (BNL),[17,18] designed to accurately describe CT states by employing a tunable range-separation parameter, γ.[17−21,23] We employed the $J^2(\gamma)$ range-separation parameter tuning scheme.[49] Finally, the electronic coupling coefficient between electronic states, V_{ba}, was obtained via the fragment-charge difference (FCD) method.[50] The effect of the solid-state environment was modeled by treating it as a dielectric medium when performing the geometry optimization of the ground and the CT states. The value of the dielectric constant used was 4.2, which is close to the value of this parameter in SubPc (3.9)[51] and C_{60} (4.0−4.5).[52−55] To this end, we employed the conductor-like polarizable continuum model (CPCM)[56] with the switching/Gaussian (SWIG) method[57−59] for surface discretization.

The FGR rate constants for the electronic transitions from the bright excited states to the (bright or dark) charge-transfer states are in the range of 0.02−27 ps^{-1} for the hollow configuration and 0.1−2.7 ps^{-1} for the on-top configuration.[34] There are many rate constants associated with the charge transfer because there are multiple bright absorbing states and dark charge-transfer states. To illustrate the overall effect of these many rates, in Figure 4 we plot the resulting total dipole moment $\mu(t)$ defined in eq 2, normalizing with respect to the steady-state dipole moment for the hollow configuration. The hollow configuration had a stronger dipole moment compared with the on-top configuration due to its stronger charge-transfer character and longer donor−acceptor separation. By fitting the dipole moment kinetics to multiexponential curves, two exponential components with rate constants of 51 and 2.0 ps^{-1} were indicated in the case of the hollow configuration. Only a single exponential with a 2.3 ps^{-1} rate constant was indicated in the case of the on-top configuration.

The FGR and classical Marcus theory charge-transfer rate constants are roughly comparable in this system,[34] which is reasonable considering the charge-transfer reaction is only barely in the inverted region.[34] However, the recombination transitions from the CT states back to the ground state occur in the far-inverted region.[34] In the hollow configuration, the recombination FGR rate constants range from approximately 10^5 to 10^8 s^{-1}, which is orders of magnitude faster than the corresponding classical Marcus theory rate constants.[34] Because we did not detect charge recombination within the time scale of our experiment, we can establish a lower bound for the charge recombination rate constant at $\sim 10^3$ s^{-1} based on our laser repetition rate (500 Hz) and the fact that we did not observe an EFISH background for $t < 0$. Meanwhile, we establish an upper bound for charge recombination at $\sim 10^8$ s^{-1} because we do not observe appreciable decay of our signal within the 150 ps time range of our experiment. Thus, the calculated FGR recombination rate constants are at least consistent with experiment.

As expected, the $k \approx 2$ ps^{-1} FGR charge-transfer rate constants are somewhat faster than the corresponding experimentally measured value, $k \approx 0.1$ ps^{-1}. This result is consistent with the view that the calculated FGR rate constants represent an upper bound for the experimentally measured rate constants. First, we note that variations in measured charge-transfer rate constants were observed from one sample to another, where differences of a factor of three were observed. Second, while our calculations ignored the possibility of long-range charge transfer, it might occur in real samples, potentially slowing down the observed charge-transfer rate. Third, the irregular shape of SubPc suggests that interfacial donor−acceptor geometries in real films would most likely deviate from the dimer optimal geometries on which the calculations were performed. Charge-transfer rates are exquisitely sensitive to geometry; minute changes in donor−acceptor distance can yield orders of magnitude changes in the charge-transfer rate. Interfacial geometries should be strongly dependent on deposition and annealing conditions. For example, for samples with the SubPc deposited on top of the C_{60}, the SubPc molecules are better able to rapidly reorient during deposition to the C_{60} molecules underneath, resulting in a stabilized configuration and faster charge transfer. Indeed, we observed charge transfer with rates as high as ~ 1 ps^{-1} for such films, as seen in Figure 3 of the Supporting Information. Fourth, charge transfer for the hollow configuration was found to follow biexponential kinetics, with fast (~ 50 ps^{-1}) and slow (~ 2 ps^{-1}) components, while charge transfer in the on-top configuration could be described by a single ~ 2 ps^{-1} rate constant. Thus, a slower CT process can be attained with samples in which the interface is dominated by the on-top configuration and where

DOI: 10.1021/jz502278k
J. Phys. Chem. Lett. 2015, 6, 569−575

the photoexcitation is tuned to selectively populate the relevant excited states.

At first glance, it appears surprising that the measured charge-transfer rate using a similar TRSHG experiment on a copper phthalocyanine (CuPc)/C_{60} heterojunction is >10 ps^{-1},[8,10] two orders of magnitude faster than our measurement of the seemingly similar SubPc/C_{60} system. However, there is not as much similarity between CuPc and SubPc heterojunctions as it would seem. CuPc films are generally polycrystalline, with preferential face-to-face stacking. The most likely configuration between CuPc and C_{60} puts the face of the CuPc extremely close to the C_{60},[10,35] enhancing charge transfer. SubPc molecules do not stack well and generally yield amorphous films. The SubPc/C_{60} interface likely exhibits a wide variety of SubPc/C_{60} configurations, dominated by configurations less optimal than the typical CuPc/C_{60} one. Therefore, we expect that the measured SubPc/C_{60} charge transfer could be much slower than CuPc/C_{60}. Indeed, the discrepancy between the CuPc/C_{60} measurements and our experiments is reduced by an order of magnitude when the SubPc/C_{60} deposition order is reversed, highlighting the importance of donor/acceptor geometry to the charge-transfer rate. Our calculations also confirm the SubPc/C_{60} heterojunction to have a one order of magnitude slower rate constant than CuPc/C_{60},[34,35] although this comparison is based on a simple dimer model where the reorientation effects previously discussed are essentially neglected.

In summary, we compared experimentally measured and theoretically predicted charge-transfer rate constants for the SubPc/C_{60} electron donor/acceptor system used in organic photovoltaics. Our combined experimental and computational study represents a first step toward understanding the complex relationship between molecular interfacial structure and charge-transfer dynamics. The experimentally measured value was $k \approx 0.1$ ps^{-1} and was seen to be highly sensitive to sample preparation, with reversed deposition order yielding ~10 times faster rates. The computational rates ranged from ~2 to 50 ps^{-1}, depending on the donor/acceptor geometry. Considering the approximations underlying the theoretical model and experimental uncertainties regarding sample preparation and spectroscopic measurements, we believe that the agreement between experiment and theory is reasonable. In addition, it is likely that charge-transfer rate constants calculated using optimal dimer geometries represent an upper bound for the experimentally measured rate constants. In particular, we find a fundamental difference in the dynamics between the two optimal geometries considered, namely, a biexponential behavior in the hollow geometry and a single exponential in the on-top geometry. Thus, measurements of the dipole moment can be used to gain insight into the dominant form of the molecular interface in an organic photovoltaic sample. Further advances of our understanding of charge-transfer dynamics in such systems toward improving the agreement between experiment and theory would require improving both the characterization of the interface structure and the modeling of the charge-transfer rates. Work toward achieving those objectives is underway in our groups.

■ ASSOCIATED CONTENT

Supporting Information

Additional experimental detail, an analysis of laser fluence, a description of the principal projection, and a discussion of the effect of altering deposition conditions. This material is available free of charge via the Internet at http://pubs.acs.org.

■ AUTHOR INFORMATION

Corresponding Author

*E-mail: jogilvie@umich.edu.

Present Address

○M.H.L.: Department of Chemistry and Centre of Scientific Computing, University of Warwick, Coventry CV4 7AL, U.K.

Notes

The authors declare no competing financial interest.

■ ACKNOWLEDGMENTS

This work was supported as part of the Center for Solar and Thermal Energy Conversion (CSTEC), an Energy Frontier Research Center funded by the U.S. Department of Energy (DOE), Office of Science, Basic Energy Sciences (BES), under award #DE-SC0000957.

■ REFERENCES

(1) Blankenship, R. E. *Molecular Mechanisms of Photosynthesis*; Wiley-Blackwell: Malden, MA, 2002.

(2) Kirkpatrick, J.; Keivanidis, P. E.; Bruno, A.; Ma, F.; Haque, S. A.; Yarstev, A.; Sundstrom, V.; Nelson, J. Ultrafast Transient Optical Studies of Charge Pair Generation and Recombination in Poly-3-hexylthiophene(P3ht):[6,6]Phenyl C_{61} Butyric Methyl Acid Ester (PCBM) Blend Films. *J. Phys. Chem. B* **2011**, *115*, 15174−15180.

(3) Etzold, F.; Howard, I. A.; Forler, N.; Cho, D. M.; Meister, M.; Mangold, H.; Shu, J.; Hansen, M. R.; Müllen, K.; Laquai, F. The Effect of Solvent Additives on Morphology and Excited-State Dynamics in PCPDTBT:PCBM Photovoltaic Blends. *J. Am. Chem. Soc.* **2012**, *134*, 10569−10583.

(4) Singh, S.; Vardeny, Z. Ultrafast Transient Spectroscopy of Polymer/Fullerene Blends for Organic Photovoltaic Applications. *Materials* **2013**, *6*, 897−910.

(5) Kandada, A. R. S.; Grancini, G.; Petrozza, A.; Perissinotto, S.; Fazzi, D.; Raavi, S. S. K.; Lanzani, G. Ultrafast Energy Transfer in Ultrathin Organic Donor/Acceptor Blend. *Sci. Rep.* **2013**, *3*, 2073.

(6) Bernardo, B.; Cheyns, D.; Verreet, B.; Schaller, R. D.; Rand, B. P.; Giebink, N. C. Delocalization and Dielectric Screening of Charge Transfer States in Organic Photovoltaic Cells. *Nat. Commun.* **2014**, *5*, 3245.

(7) Magyar, R. J.; Tretiak, S. Dependence of Spurious Charge-Transfer Excited States on Orbital Exchange in TDDFT: Large Molecules and Clusters. *J. Chem. Theory Comput.* **2007**, *3*, 976−987.

(8) Kaake, L. G.; Jailaubekov, A.; Williams, K. J.; Zhu, X.-Y. Probing Ultrafast Charge Separation at Organic Donor/Acceptor Interfaces by a Femtosecond Electric Field Meter. *Appl. Phys. Lett.* **2011**, *99*, 083307.

(9) Amarasinghe Vithanage, D.; Devižis, A.; Abramavičius, V.; Infahsaeng, Y.; Abramavičius, D.; MacKenzie, R. C. I.; Keivanidis, P. E.; Yartsev, A.; Hertel, D.; Nelson, J.; et al. Visualizing Charge Separation in Bulk Heterojunction Organic Solar Cells. *Nat. Commun.* **2013**, *4*, 2334.

(10) Jailaubekov, A. E.; Willard, A. P.; Tritsch, J. R.; Chan, W.-L.; Sai, N.; Gearba, R.; Kaake, L. G.; Williams, K. J.; Leung, K.; Rossky, P. J.; et al. Hot Charge-Transfer Excitons Set the Time Limit for Charge Separation at Donor/Acceptor Interfaces in Organic Photovoltaics. *Nat. Mater.* **2013**, *12*, 66−73.

(11) Boyd, R. W. *Nonlinear Optics*, 3rd ed.; Academic Press: Burlington, MA, 2008.

(12) Baumeier, B.; Andrienko, D.; Rohlfing, M. Frenkel and Charge-Transfer Excitations in Donor-Acceptor Complexes from Many-Body Green'S Functions theory. *J. Chem. Theory Comput.* **2012**, *8*, 2790−2795.

DOI: 10.1021/jz502278k
J. Phys. Chem. Lett. 2015, 6, 569−575

(13) Duchemin, I.; Deutsch, T.; Blase, X. Short-Range to Long-Range Charge-Transfer Excitations in the Zincbacteriochlorin-Bacteriochlorin Complex: A Bethe-Salpeter Study. *Phys. Rev. Lett.* **2012**, *109*, 167801.
(14) Garcia-Lastra, J. M.; Thygesen, K. S. Renormalization of Optical Excitations in Molecules near a Metal Surface. *Phys. Rev. Lett.* **2011**, *106*, 187402.
(15) Blase, X.; Attaccalite, C. Charge-Transfer Excitations in Molecular Donor-Acceptor Complexes within the Many-Body Bethe-Salpeter Approach. *Appl. Phys. Lett.* **2011**, *99*, 171909.
(16) Dreuw, A.; Weisman, J. L.; Head-Gordon, M. Long-Range Charge-Transfer Excited States in Time-Dependent Density Functional Theory Require Non-Local Exchange. *J. Chem. Phys.* **2003**, *119*, 2943−2946.
(17) Baer, R.; Neuhauser, D. Density Functional Theory with Correct Long-Range Asymptotic Behavior. *Phys. Rev. Lett.* **2005**, *94*, 043002.
(18) Livshits, E.; Baer, R. a Well-Tempered Density Functional Theory of Electrons in Molecules. *Phys. Chem. Chem. Phys.* **2007**, *9*, 2932−2941.
(19) Stein, T.; Kronik, L.; Baer, R. Reliable Prediction of Charge Transfer Excitations in Molecular Complexes Using Time-Dependent Density Functional Theory. *J. Am. Chem. Soc.* **2009**, *131*, 2818−2820.
(20) Stein, T.; Eisenberg, H.; Kronik, L.; Baer, R. Fundamental Gaps in Finite Systems from Eigenvalues of a Generalized Kohn-Sham Method. *Phys. Rev. Lett.* **2010**, *105*, 266802.
(21) Stein, T.; Kronik, L.; Baer, R. Prediction of Charge-Transfer Excitations in Coumarin-Based Dyes Using a Range-Separated Functional Tuned from First Principles. *J. Chem. Phys.* **2009**, *131*, 244119.
(22) Manna, A. K.; Dunietz, B. D. Communication: Charge-Transfer Rate Constants in Zinc-Porphyrin-Porphyrin-Derived Dyads: A Fermi Golden Rule First-Principles-Based Study. *J. Chem. Phys.* **2014**, *141*, 121102.
(23) Zheng, S.; Phillips, H.; Geva, E.; Dunietz, B. D. Ab Initio Study of the Emissive Charge-Transfer States of Solvated Chromophore-Functionalized Silsesquioxanes. *J. Am. Chem. Soc.* **2012**, *134*, 6944−6947.
(24) Zheng, S.; Geva, E.; Dunietz, B. D. Solvated Charge Transfer States of Functionalized Anthracene and Tetracyanoethylene Dimers: A Computational Study Based on a Range Separated Hybrid Functional and Charge Constrained Self-Consistent Field with Switching Gaussian Polarized Continuum Models. *J. Chem. Theory Comput.* **2013**, *9*, 1125−1131.
(25) Phillips, H.; Zheng, Z.; Geva, E.; Dunietz, B. D. Orbital Gap Predictions for Rational Design of Organic Photovoltaic Materials. *Org. Electron.* **2014**, *15*, 1509−1520.
(26) Yi, Y.; Coropceanu, V.; Brédas, J.-L. Exciton-Dissociation and Charge-Recombination Processes in Pentacene/C_{60} Solar Cells: Theoretical Insight Into The Impact Of Interface Geometry. *J. Am. Chem. Soc.* **2009**, *131*, 15777−15783.
(27) Yi, Y.; Coropceanu, V.; Brédas, J.-L. A Comparative Theoretical Study of Exciton-Dissociation and Charge-Recombination Processes in Oligothiophene/Fullerene and Oligothiophene/Perylenediimide Complexes for Organic Solar Cells. *J. Mater. Chem.* **2011**, *21*, 1479−1486.
(28) Zhugayevych, A.; Postupna, O.; Bakus, R. C., II; Welch, G. C.; Bazan, G. C.; Tretiak, S. Ab Initio Study of a Molecular Crystal for Photovoltaics: Light Absorption, Exciton and Charge Carrier Transport. *J. Phys. Chem. C* **2013**, *117*, 4920−4930.
(29) Leng, C.; Qin, H.; Si, Y.; Zhao, Y. Theoretical Prediction of the Rate Constants for Exciton Dissociation and Charge Recombination to a Triplet State in PCPDTBT with Different Fullerene Derivatives. *J. Phys. Chem. C* **2014**, *118*, 1843−1855.
(30) Marcus, R. A. On the Theory of Oxidation-Reduction Reactions Involving Electron Transfer. I. *J. Chem. Phys.* **1956**, *24*, 966−978.
(31) Marcus, R. A. Electrostatic Free Energy and Other Properties of States Having Nonequilibrium Polarization. I. *J. Chem. Phys.* **1956**, *24*, 979−989.
(32) Marcus, R. A. Electron Transfer Reactions in Chemistry. Theory and Experiment. *Rev. Mod. Phys.* **1993**, *65*, 599−610.
(33) Lee, M. H.; Dunietz, B. D.; Geva, E. Calculation from First Principles of Intramolecular Golden-Rule Rate Constants for Photo-Induced Electron Transfer in Molecular Donor-Acceptor Systems. *J. Phys. Chem. C* **2013**, *117*, 23391−23401.
(34) Lee, M. H.; Geva, E.; Dunietz, B. D. Calculation from First-Principles of Golden Rule Rate Constants for Photoinduced Subphthalocyanine/Fullerene Interfacial Charge Transfer and Recombination in Organic Photovoltaic Cells. *J. Phys. Chem. C* **2014**, *118*, 9780−9789.
(35) Lee, M. H.; Dunietz, B. D.; Geva, E. Donor-to-Donor vs Donor-to-Acceptor Interfacial Charge Transfer States in the Phthalocyanine-Fullerene Organic Photovoltaic System. *J. Phys. Chem. Lett.* **2014**, *5*, 3810−3816.
(36) Nitzan, A. *Chemical Dynamics in Condensed Phases*; Oxford University Press: New York, 2006.
(37) Kestner, N. R.; Logan, J.; Jortner, J. Thermal Electron Transfer Reactions in Polar Solvents. *J. Phys. Chem.-US* **1974**, *78*, 2148−2166.
(38) Jortner, J.; Bixon, M. Intramolecular Vibrational Excitations Accompanying Solvent-Controlled Electron Transfer Reactions. *J. Chem. Phys.* **1988**, *88*, 167−170.
(39) Coalson, R. D.; Evans, D. G.; Nitzan, A. A Nonequilibrium Golden Rule Formula for Electronic State Populations in Nonadiabatically Coupled Systems. *J. Chem. Phys.* **1994**, *101*, 436−448.
(40) Leggett, A.; Chakravarty, S.; Dorsey, A.; Fisher, M.; Garg, A.; Zwerger, W. Dynamics of the Dissipative Two-State System. *Rev. Mod. Phys.* **1987**, *59*, 1−85.
(41) De Vault, D.; Chance, B. Studies of Photosynthesis Using a Pulsed Laser: I. Temperature Dependence of Cytochrome Oxidation Rate in Chromatium. Evidence for Tunneling. *Biophys. J.* **1966**, *6*, 825−847.
(42) Barbara, P. F.; Meyer, T. J.; Ratner, M. A. Contemporary Issues in Electron Transfer Research. *J. Phys. Chem.* **1996**, *100*, 13148−13168.
(43) Wilcox, D. E.; Sykes, M. E.; Niedringhaus, A.; Shtein, M.; Ogilvie, J. P. Heterodyne-Detected and Ultrafast Time-Resolved Second-Harmonic Generation for Sensitive Measurements of Charge Transfer. *Opt. Lett.* **2014**, *39*, 4274−4277.
(44) Oliphant, T. E. Python for Scientific Computing. *Comput. Sci. Eng.* **2007**, *9*, 10−20.
(45) Huang, K.; Rhys, A. Theory of Light Absorption and Non-Radiative Transitions in F-Centres. *Proc. R. Soc. London, Ser. A* **1950**, *204*, 406−423.
(46) Wu, Q.; Van Voorhis, T. Direct Optimization Method to Study Constrained Systems within Density-Functional theory. *Phys. Rev. A* **2005**, *72*, 024502.
(47) Chai, J.-D.; Head-Gordon, M. Systematic Optimization of Long-Range Corrected Hybrid Density Functionals. *J. Chem. Phys.* **2008**, *128*, 084106.
(48) Chai, J.-D.; Head-Gordon, M. Long-Range Corrected Hybrid Density Functionals with Damped Atom-Atom Dispersion Corrections. *Phys. Chem. Chem. Phys.* **2008**, *10*, 6615−6620.
(49) Kuritz, N.; Stein, T.; Baer, R.; Kronik, L. Charge-Transfer-Like $\pi \rightarrow \pi^*$ Excitations in Time-Dependent Density Functional Theory: A Conundrum and Its Solution. *J. Chem. Theory Comput.* **2011**, *7*, 2408−2415.
(50) Voityuk, A. A.; Rösch, N. Fragment Charge Difference Method for Estimating Donor-Acceptor Electronic Coupling: Application to DNA π-Stacks. *J. Chem. Phys.* **2002**, *117*, 5607−5616.
(51) Gommans, H.; Cheyns, D.; Aernouts, T.; Girotto, C.; Poortmans, J.; Heremans, P. Electro-Optical Study of Subphthalocyanine in a Bilayer Organic Solar Cell. *Adv. Funct. Mater.* **2007**, *17*, 2653−2658.
(52) Hebard, A. F.; Haddon, R. C.; Fleming, R. M.; Kortan, A. R. Deposition and Characterization of Fullerene Films. *Appl. Phys. Lett.* **1991**, *59*, 2109−2111.
(53) Pevzner, B.; Hebard, A. F.; Dresselhaus, M. S. Role of Molecular Oxygen and Other Impurities in the Electrical Transport and

DOI: 10.1021/jz502278k
J. Phys. Chem. Lett. 2015, 6, 569−575

Dielectric Properties of C_{60} Films. *Phys. Rev. B* **1997**, *55*, 16439−16449.
(54) Dutton, G. J.; Robey, S. W. Exciton Dynamics at CuPc/C_{60} Interfaces: Energy Dependence of Exciton Dissociation. *J. Phys. Chem. C* **2012**, *116*, 19173−19181.
(55) Pandey, R.; Gunawan, A. A.; Mkhoyan, K. A.; Holmes, R. J. Efficient Organic Photovoltaic Cells Based on Nanocrystalline Mixtures of Boron Subphthalocyanine Chloride and C_{60}. *Adv. Funct. Mater.* **2012**, *22*, 617−624.
(56) Cossi, M.; Rega, N.; Scalmani, G.; Barone, V. Energies, Structures, And Electronic Properties of Molecules in Solution with the C-PCM Solvation Model. *J. Comput. Chem.* **2003**, *24*, 669−681.
(57) Lange, A. W.; Herbert, J. M. Polarizable Continuum Reaction-Field Solvation Models Affording Smooth Potential Energy Surfaces. *J. Phys. Chem. Lett.* **2010**, *1*, 556−561.
(58) Lange, A. W.; Herbert, J. M. A Smooth, Nonsingular, And Faithful Discretization Scheme for Polarizable Continuum Models: The Switching/Gaussian Approach. *J. Chem. Phys.* **2010**, *133*, 244111.
(59) York, D. M.; Karplus, M. A Smooth Solvation Potential Based on the Conductor-Like Screening Model. *J. Phys. Chem. A* **1999**, *103*, 11060−11079.

DOI: 10.1021/jz502278k
J. Phys. Chem. Lett. 2015, 6, 569−575